Sustainable Energy & Fuels

PAPER

View Article Online
View Journal | View Issue

Cite this: *Sustainable Energy Fuels*, 2019, **3**, 2087

Highly efficient fullerene and non-fullerene based ternary organic solar cells incorporating a new tetrathiocin-cored semiconductor†

Lethy Krishnan Jagadamma,[a] Rupert G. D. Taylor,[b] Alexander L. Kanibolotsky,[cd] Muhammad Tariq Sajjad,[a] Iain A. Wright,‡[b] Peter N. Horton,[e] Simon J. Coles,[e] Ifor D. W. Samuel*[a] and Peter J. Skabara*[c]

Received 1st June 2019
Accepted 3rd June 2019

DOI: 10.1039/c9se00343f

rsc.li/sustainable-energy

A new dual-chain oligothiophene-based organic semiconductor, **EH-5T-TTC**, is presented. The molecule contains two conjugated chains linked by a fused tetrathiocin core. X-ray crystallography reveals a boat conformation within the 8-membered sulfur heterocycle core and extensive π–π and intermolecular sulfur–sulfur interactions in the bulk, leading to a 2-dimensional structure. This unusual molecule has been studied as a ternary component in organic solar cell blends containing the electron donor **PTB7-Th** and both fullerene ($PC_{71}BM$) and non-fullerene acceptors **ITIC** and **EH-IDTBR**. By incorporating **EH-5T-TTC** as a ternary component, the power conversion efficiency of the binary blends containing non-fullerene acceptor increases by 17% (from 7.8% to 9.2%) and by 85% for the binary blend with fullerene acceptor (from 3.3% to 6.3%). Detailed characterisation of the ternary blend systems implies that the ternary small molecule **EH-5T-TTC** functions differently in polymer:fullerene and polymer:non-fullerene blends and has dual functions of morphology modification and complementary spectral absorption.

Introduction

Organic photovoltaic (OPV) devices based on nanocomposites of π-conjugated semiconductors are a prospective solar cell technology[1] and have attracted considerable attention due to unprecedented attributes such as printability, foldability, portability, wearability, semi-transparency and amenability to cost-effective large area fabrication.[2] Extensive and focussed research to enhance the power conversion efficiency (PCE) of organic solar cells have led to the development of highly efficient bulk heterojunction (BHJ) single and multijunction organic solar cells with PCEs > 15%.[3–8] This has been achieved through the development of new photoactive materials, interfacial modification and device architecture design. The power conversion efficiency of solar cells is determined mainly by three performance parameters of open circuit voltage (V_{OC}), fill factor (FF) and short circuit current density (J_{SC}). Even though these parameters are complexly interrelated, each of them is directly influenced by some specific properties of the donor/acceptor (D/A) components constituting the active layer. V_{OC} is primarily determined by the energy gap between the donor HOMO and acceptor LUMO, FF is affected by the D/A morphology and carrier mobility and the J_{SC} by the light absorption properties of the D/A blend active layer. One simple approach to enhance the efficiency of OPVs is to extend the spectral range of light absorption by the photosensitive active layer.

Despite the high absorption coefficient of π-conjugated organic semiconductors (10^5–10^6 cm^{-1}), due to their bonding properties, the narrow absorption bandwidth of the organic semiconductors limit the spectral overlap of the D/A blend with the solar spectrum, thus adversely restricting the J_{SC}.[9] Furthermore, the low exciton diffusion length (5–15 nm) and low charge carrier mobility (~10^{-4} cm^2 V^{-1} s^{-1}) of organic semiconductors restrict the active layer thickness of the BHJ solar cells ~80–150 nm, which also results in incomplete absorption of the incident solar spectrum. To circumvent this, homo and heterojunction tandem solar cell device architectures can be introduced to broaden the light harvesting spectral region and to reduce any thermalisation losses.[10] Although the technology

[a]*Organic Semiconductor Centre, SUPA, School of Physics and Astronomy, University of St. Andrews, St. Andrews, Fife, KY16 9SS, UK. E-mail: idws@st-andrews.ac.uk*

[b]*WestCHEM, Department of Pure and Applied Chemistry, University of Strathclyde, 295 Cathedral Street, Glasgow, G1 1XL, UK*

[c]*WestCHEM, School of Chemistry, University of Glasgow, Glasgow, G12 8QQ, UK. E-mail: peter.skabara@glasgow.ac.uk*

[d]*Institute of Physical-Organic Chemistry and Coal Chemistry, Kyiv 02160, Ukraine*

[e]*School of Chemistry, University of Southampton, Highfield, Southampton, SO17 1BJ, UK*

† Electronic supplementary information (ESI) available: General experimental and synthetic and crystallography details; AFM images, spectroscopic data and device data. CCDC 1856815. For ESI and crystallographic data in CIF or other electronic format see DOI: 10.1039/c9se00343f. Additional supporting data are accessible from http://dx.doi.org/10.5525/gla.researchdata.833

‡ Present address: Department of Chemistry, Loughborough University, Loughborough LE11 3TU, UK.

is successful in terms of achieving its purpose, the improvement in PCE comes with a high cost and complexity. The design of charge recombination layers, stringent current matching conditions, necessity of solvents with orthogonal solubility properties, complex fabrication steps and low yield, all make the tandem architecture too complicated for a printing process and hence less appealing for adoption by industry.[2] Another very promising and simple strategy is to keep the single junction architecture, but combine multiple donor/acceptor molecules to extend the spectral overlap of the organic solar cells with the incident solar spectrum, resulting in so-called ternary blend organic solar cells.[11] Here, in this work, this latter approach has been used to obtain highly efficient fullerene and non-fullerene based ternary organic solar cells; the light absorbing active layer is composed of two donor materials and one fullerene/non-fullerene acceptor molecule and such ternary blend systems have been shown to provide significant improvements in power conversion efficiencies when compared to parent binary blends.[11,12]

The main donor material considered is the polymer poly[4,8-bis(5-(2-ethylhexyl)thiophen-2-yl)benzo[1,2-*b*;4,5-*b*′]dithiophene-2,6-diyl-*alt*-(4-(2-ethylhexyl)-3-fluorothieno[3,4-*b*]thiophene)-2-(carboxylate-2-6-diyl)] (**PTB7-Th**), chosen due to its high absorption properties and compatibility with both fullerene and non-fullerene acceptors.[3,5] The ternary donor molecule considered is a novel small molecule: **EH-5T-TTC**, [1,3,6,8-tetrakis(3′-(2-ethylhexyl)-5′-methyl-[2,2′-bithiophen]-5-yl)dithieno[3,4-*c*:3′,4′-*g*][1,2,5,6]tetrathiocin]. In a ternary solar cell, the third component enhances the efficiency of the binary host system either by energy transfer or by charge transfer leading to an increase in short circuit current density by extended absorption and increased exciton/charge generation.[13,14] A ternary component can also modify the morphology of the binary host blend by increasing the D/A interfacial area for exciton dissociation and forming extended, interpenetrating networks of donor/acceptor domains to facilitate charge transport. However, there are challenges in obtaining efficient ternary blend OPVs. Choosing a compatible ternary component that can be loaded in a sufficient amount into the binary host system, so as to increase the absorption in the complementary spectral range without disrupting the host blend morphology, is a challenging issue. Previously, Yang *et al.*[15] and Thompson *et al.*[16,17] reported that similarity in properties such as surface energy, chemical structure, molecular orientation, crystallite and domain size are necessary for a compatible ternary component. However, recently Mai *et al.*[18] relaxed the condition of molecular structural similarity and demonstrated that morphology compatibility in terms of molecular packing and phase separation is the key to the ternary component selection.

In the present study, the binary blend systems investigated to enhance the power conversion efficiency are **PTB7-Th:ITIC** [3,9-bis(2-methylene-(3-(1,1-dicyanomethylene)-indanone))-5,5,11,11-tetrakis(4-hexylphenyl)-dithieno[2,3-*d*:2′,3′-*d*′]-*s*-indaceno[1,2-*b*:5,6-*b*′]dithiophene], **PTB7-Th:EH-IDTBR** and **PTB7-**

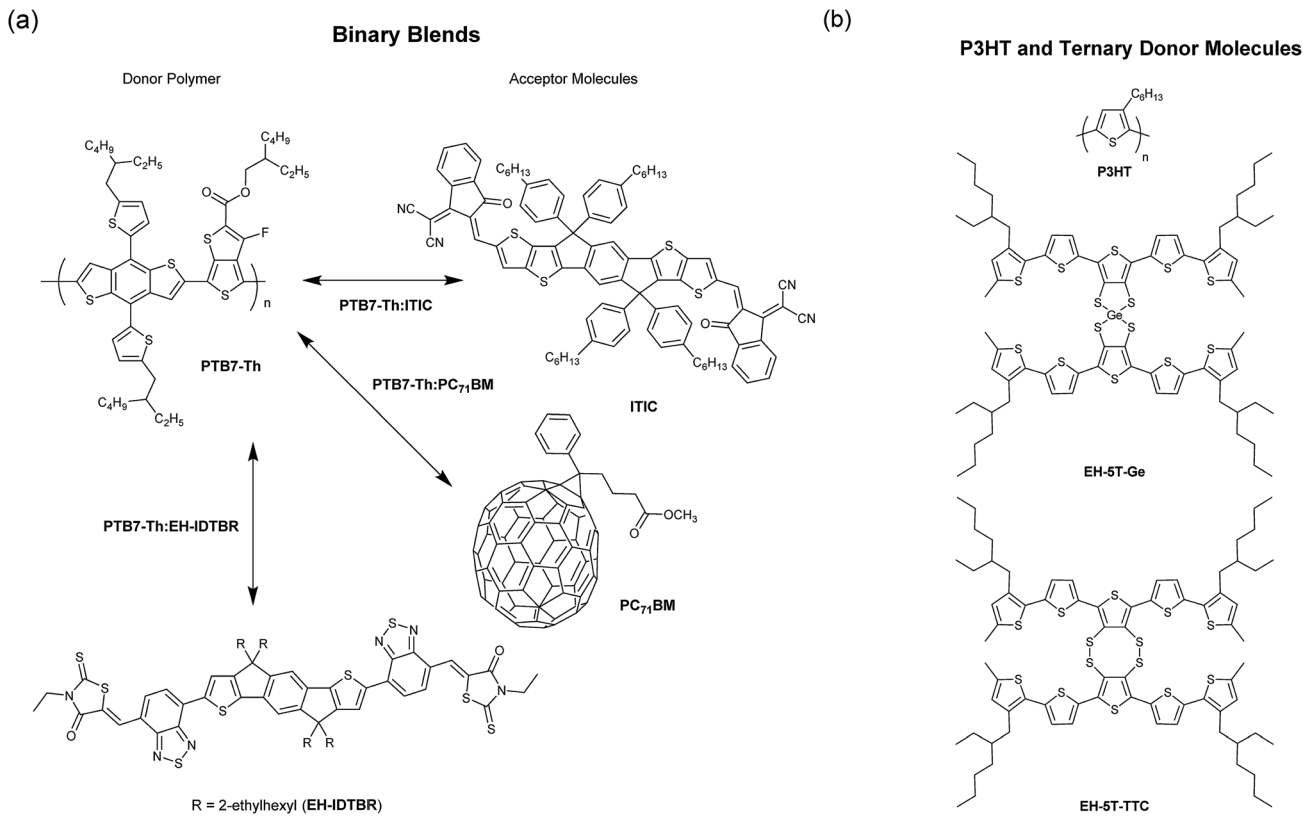

Scheme 1 (a) Molecular structures of the binary blends and (b) P3HT and the ternary components considered in this work.

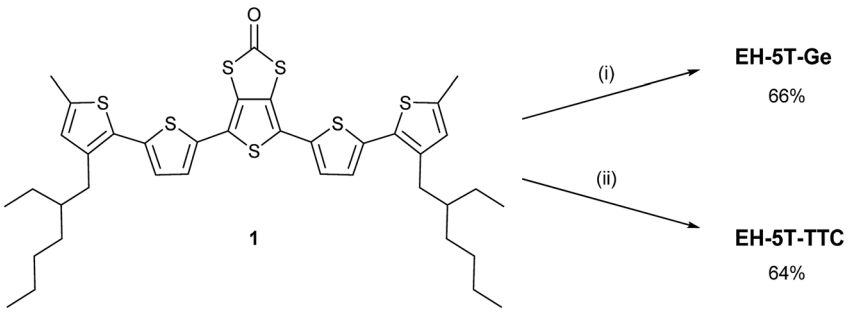

Scheme 2 Reagents and conditions: (i) NaOMe, THF, then $GeBr_4$, (ii) NaOMe, THF, then I_2.

Th:PC_{71}BM. Molecular structures of these molecules are shown in Scheme 1. The selected donor materials **EH-5T-TTC**, **EH-5T-Ge** [4,4′,6,6′-tetrakis(3′-(2-ethylhexyl)-5′-methyl-[2,2′-bithiophen]-5-yl)-2,2′-spirobi[thieno[3,4-*d*][1,3,2]dithiagermole]] and **P3HT** [poly(3-hexylthiophene-2,5-diyl)] are presented initially as potential candidates for ternary devices, with complementary absorption properties with respect to the binary systems considered. The materials **P3HT** and **EH-5T-Ge** were chosen simply to compare the main subject of this work (**EH-5T-TTC**), with a well-known donor polymer and a close structural analogue, respectively. By introducing the ternary donor component **EH-5T-TTC** into BHJ OPV devices, the PCE of the binary blend systems increased by ~7% (7.2 to 7.7%) for **PTB7-Th:ITIC**, ~85% for **PTB7-Th:PC_{71}BM** (3.3% to 6.3%) and ~17% (7.8 to 9.2%) for **PTB7-Th:EH-IDTBR**. The good generality of the ternary component **EH-5T-TTC** to both fullerene and non-fullerene based organic solar cells is significant and such wide applicability has seldom been reported in ternary blend organic solar cells. Detailed characterisation of the ternary blend systems implies that the ternary small molecule **EH-5T-TTC** functions differently in polymer:fullerene and polymer:non-fullerene blends and has dual function in terms of morphology modification and complementary spectral absorption. The improvement in PCE of the ternary blend systems due to the incorporation of **EH-5T-TTC** is a synergistic effect of enhanced light absorption, improved nanoscale and percolative morphology, reduced recombination losses and increased exciton generation and dissociation probability.

Synthesis of EH-5T-TTC and X-ray crystallographic studies

The syntheses of compounds **EH-5T-TTC** and **EH-5T-Ge** are accomplished from the 1,3-dithiole-2-one precursor (**1** in Scheme 2), which in turn is prepared from a protocol reported in our previous work on a hexyl analogue of **EH-5T-Ge**[19] and utilises aryl aldehydes for the construction of conjugated oligomers with a fused 1,3-dithiole-2-one heterocycle.[20] The full experimental details and characterisation of all new compounds are provided in the ESI section.† The treatment of compound **1** in THF with sodium methoxide removes the carbonyl functionality to give the corresponding dithiolate; this intermediate can then be reacted with $GeBr_4$ or iodine to give compounds **EH-5T-Ge** and **EH-5T-TTC**, respectively. In the case of **EH-5T-TTC**, this is the first time that a tetrathiocin core unit has been introduced into a conjugated oligomer structure and the fascinating structural and packing features resulting from this dual-chain molecule are discussed below.

The molecular structure of **EH-5T-TTC**, determined by single crystal diffractions studies, is shown in Fig. 1. The asymmetric unit is represented by the half-unit formed by the scission drawn in the figure (dashed line). The complete molecule is

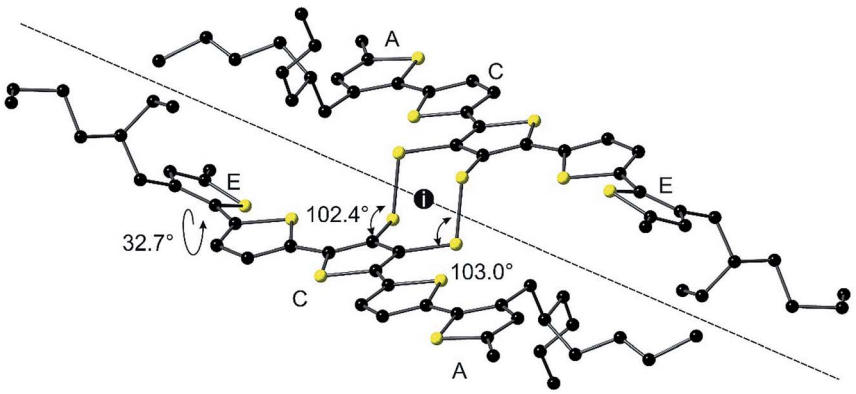

Fig. 1 Molecular structure of EH-5T-TTC with hydrogens omitted for clarity. The inversion centre of the asymmetric unit is marked with the letter i.

therefore generated by an inversion centre positioned in the middle of the 8-membered tetrathiocin ring. This heterocycle forms a boat conformer with a dihedral angle of 74.60(12)° (measured between planes of C–S–S–C and S–S–S–S) and C–S–S angles of 102.38(14)° and 103.03(13)°. The thiophenes in the oligomer chains retain good planarity across 5 units, with torsion angles (S–C–C–S) in the range 174.3(2)–179.6(2)°. However, one terminal thiophene is twisted with respect to the remainder of the chain, adopting a *syn* conformer with the neighbouring ring with a torsion angle of 32.7(4)°. Such a deviation in planarity by a terminal thiophene has been observed in our previous work on related septithiophene[21] and quinquithiophene[19] dual-chain structures. The stability of the disulfide bridges is inferred by the S–S bond lengths in the structure. The covalent radius of S is stated to be typically in the range of 1.03 Å to 1.05 Å and in ring systems the S–S bond length is quoted as up to 2.10 Å.[22] In **EH-5T-TTC**, the corresponding bond length is 2.0851(15) Å and therefore indicates a stable disulfide bond.

The molecular packing observed in **EH-5T-TTC** consists of π–π interactions within both sets of quinquithiophene chains in a slip-stacked arrangement (Fig. 2(a) and (b)), such that the coplanar terminal thiophene (E in Fig. 1), resides over the central thiophene ring (C) in the molecule above (and below) it with an inter-ring distance of 3.451(3) Å. Each of the stacks feature close intermolecular S···S contacts (Fig. 2(a) and (c)). These interactions are 3.4815(17) Å apart (sum of the van der Waals radii for two sulfurs is 3.6 Å), and involve the sulfur atom of the central thiophene ring and the sulfur atom of the twisted terminal thiophene (ring A in Fig. 1). Because of the nature of the slip-stacked structure, these S···S contacts perpetuate through the crystal. In combination with the π–π interactions, these contacts give rise to a structure featuring extensive 2-dimensional orbital overlap which is important for good charge transport properties in the bulk.[23] Note that the sheets depicted in Fig. 2(a) are insulated by the alkyl chains, which impedes the material from achieving a 3-dimensional network of close contacts.

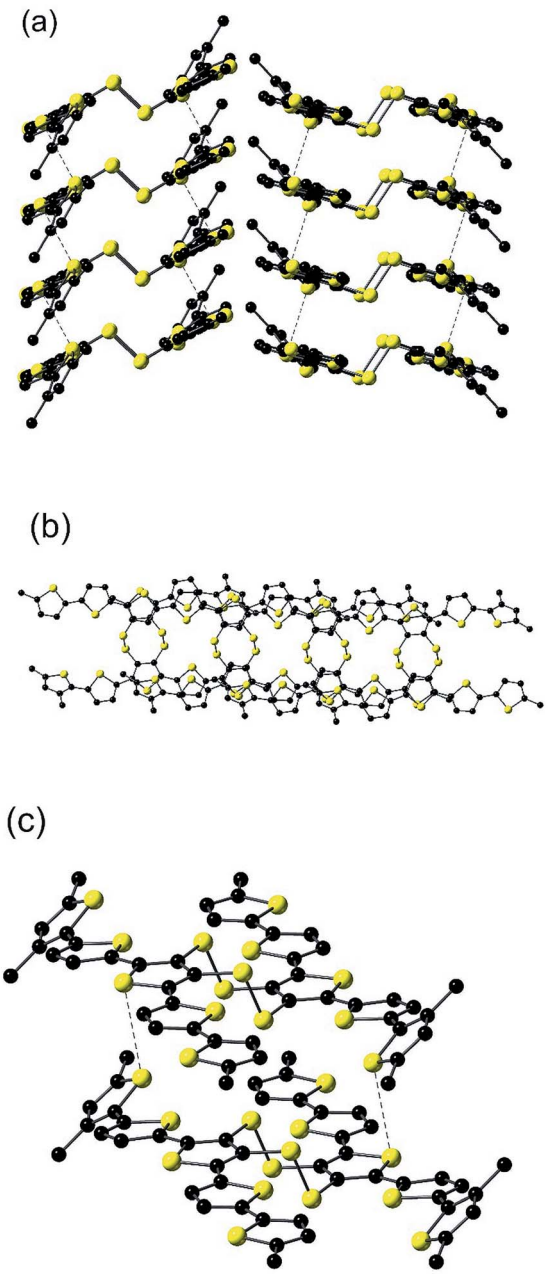

Fig. 2 Packing diagrams of EH-5T-TTC with the ethylhexyl chains truncated for ease of viewing. The dashed lines represent S···S close contacts. Figure (a) shows sulfur contacts within stacks of molecules, (b) shows the slip-stacked arrangement and (c) clearly depicts the chalcogen interactions between a pair of molecules.

Photophysical and photovoltaic studies of blends

The first series of blends to be studied incorporated **PTB7-Th** as the donor and **ITIC** as the acceptor component. The UV-vis absorption spectra of the donor, acceptor and the corresponding binary blend (**PTB7-Th:ITIC**) films are shown in Fig. 3(a) (see also Fig. S1† for energy level diagrams of the individual components in the binary and each of the ternary configurations). The absorption of the **PTB7-Th:ITIC** blend is mainly concentrated in the 550–750 nm spectral range, with poor absorption below the wavelength of 550 nm. Fig. 3(b) shows the absorption spectra of the three selected ternary component molecules of **P3HT**, **EH-5T-Ge** and **EH-5T-TTC** and for these molecules the absorption is mainly concentrated in the 400–600 nm wavelength range, thus giving complementary absorption to the **PTB7-Th** donor molecule. The energy level diagrams of the **PTB7-Th:ITIC** blend alongside each ternary component, **P3HT**, **EH-5T-Ge** and **EH-5T-TTC**, are shown in Fig. 3(c). The diagram shows that the energy level alignment should support energy/charge transfer across the series of potential ternary components. Further, the photoluminescence (PL) spectra of the ternary components have good overlap with the binary blend absorption spectra (Fig. 3(d)), which is also a criterion for favourable energy transfer to occur.

Since the conditions of complementary absorption and energy transfer are satisfied for the three selected ternary donor

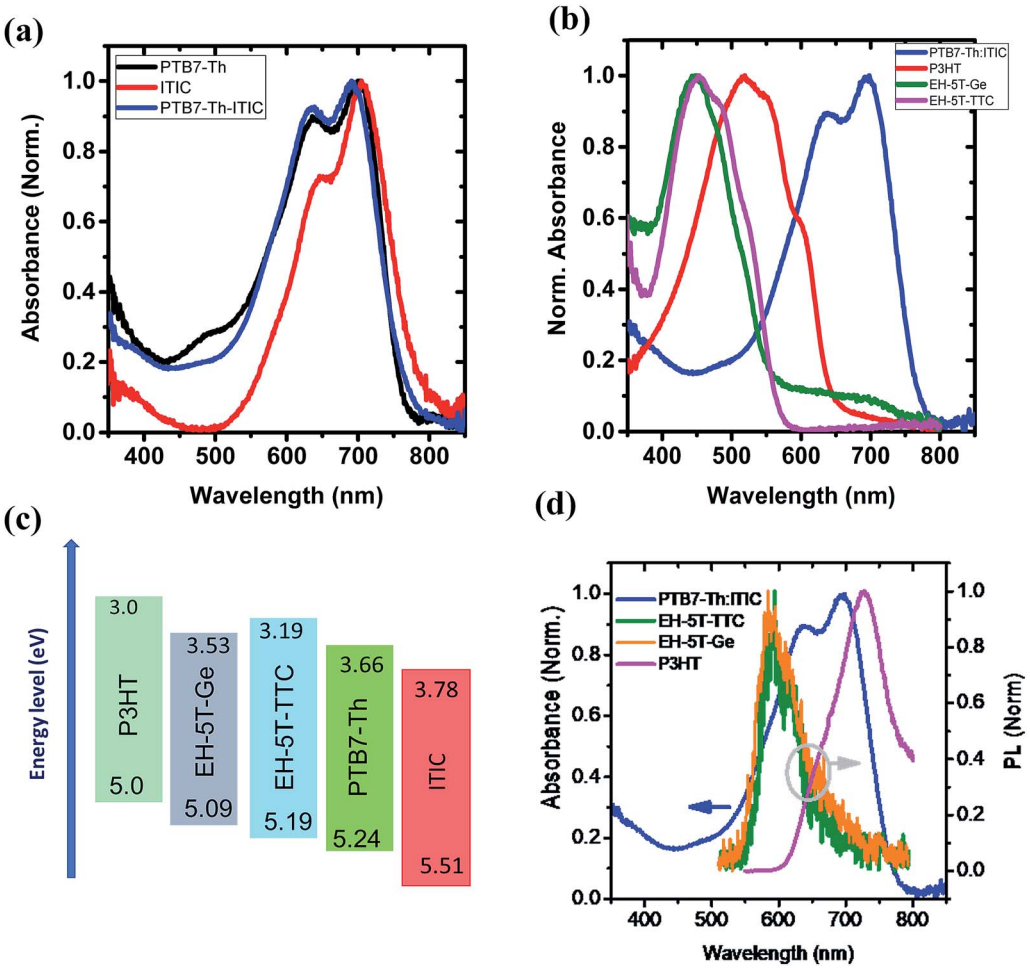

Fig. 3 (a) UV-vis absorption spectrum of the **PTB7-Th:ITIC** binary blend system and spectra of the individual components; (b) complementary UV-vis absorption properties of the ternary component donor molecules and the binary **PTB7-Th:ITIC** blend; (c) energy level diagram of the **PTB7-Th**, **ITIC** and its ternary donor components; (d) PL spectra of the ternary donor components and the absorption spectra of the binary blend film.

molecules, solar cells were fabricated to investigate their influence on power conversion efficiency. The OPV device architecture considered was the inverted configuration, consisting of ITO/ZnO/active layer blend/MoO_3/Ag. Among the three ternary components tested, only the ternary blend system consisting of **EH-5T-TTC** has shown an improvement in PCE (Fig. S2†). For the ternary blend system consisting of **P3HT** and **EH-5T-Ge** a drastic drop in PCE is observed. This could be due to the surface energy differences among the components leading to their poor miscibility and/or incompatible crystalline structure or orientation. The PCE comparison of the ternary blends with the binary blends and the corresponding *J*–*V* characteristics are shown in Fig. S2.† Since the ternary blend system consisting of **EH-5T-TTC** showed an enhancement in PCE, the optimum content of **EH-5T-TTC** was investigated. Fig. S3† shows the development of the absorption spectrum of the ternary blend as the loading of **EH-5T-TTC** increases. As the amount of the ternary component **EH-5T-TTC** increases in the **PTB7-Th:ITIC** blend, the absorption in the 400–600 nm wavelength range also increases. The corresponding effect on the photovoltaic performance parameters are shown in Fig. 4. The figure shows that a 10% composition of **EH-5T-TTC** achieves the highest PCE of the ternary blends studied (0–40 wt% composition), with an improvement to 7.7% PCE, compared to 7.2% for the binary blend which does not contain **EH-5T-TTC**. This increase is achieved through the improvement of the short circuit current density, despite losses in the values of the open circuit voltage and fill factor. The increase in J_{SC} could be explained by the improved light harvesting properties of the ternary blend and this is supported by the improved EQE in the 10% ternary blend compared with the binary blend (Fig. 4(c)). Moreover, the improved EQE is mainly in the 400–600 nm wavelength range, where the absorption due to the ternary component has shown an improvement in Fig. S3.†

With the promising PCE enhancement observed for the **PTB7-Th:ITIC** blend with the incorporation of **EH-5T-TTC**, another ternary blend OPV system was fabricated by replacing **ITIC** with **EH-IDTBR**. The UV-vis absorption spectrum of the **PTB7-Th:EH-IDTBR** blend is shown in Fig. 5(a) and the absorption is mainly concentrated in the 500–750 nm

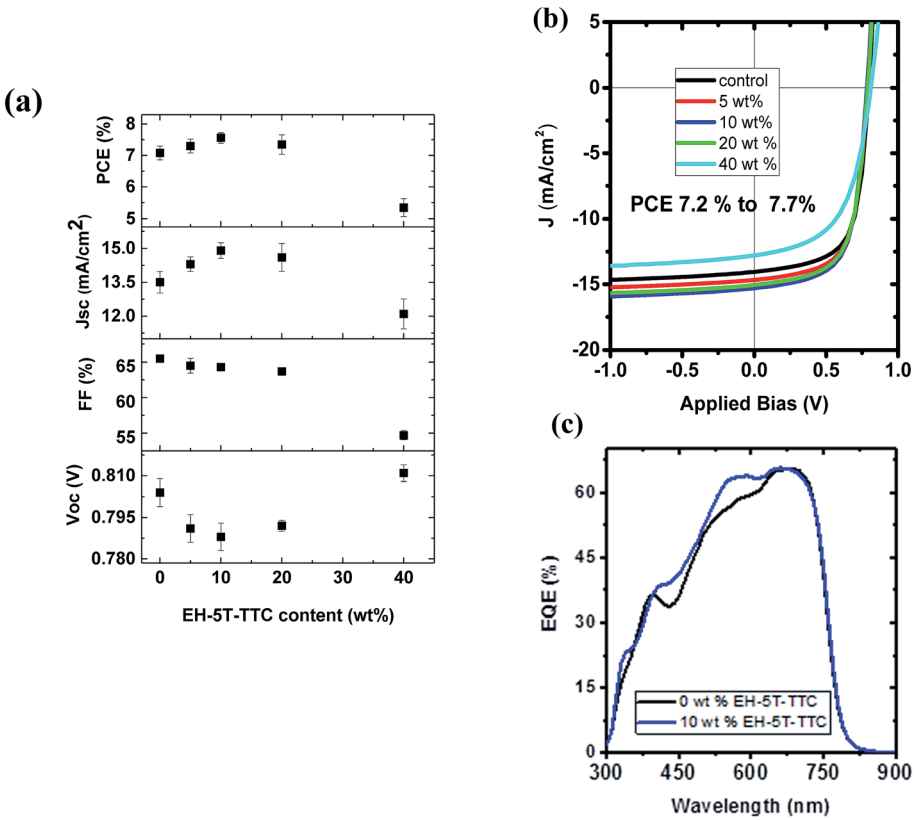

Fig. 4 (a) Optimisation of **EH-5T-TTC** content in the **PTB7-Th:ITIC** blend system. The corresponding *J*–*V* characteristics and EQE spectra are shown in (b) and (c). The OPV device performance parameters are shown for 8–10 devices.

wavelength range with poor absorption for wavelengths below 500 nm. With the incorporation of 10 wt% **EH-5T-TTC** the absorption of the binary blend **PTB7-Th:EH-IDTBR** for the spectral range below 500 nm is enhanced. The energy level diagram is shown in Fig. 5(b) and the band positions are favourable for the charge transfer and/or exciton transfer to occur. The comparison of the *J*–*V* characteristics corresponding to the binary **PTB7-Th:EH-IDTBR** and the ternary **EH-5T-TTC:PTB7-Th:EH-IDTBR** blend systems are shown in Fig. 5(c). The corresponding photovoltaic performance parameters are listed in Table S1.† It was found that the addition of 10 wt% **EH-5T-TTC** to the **PTB7-Th:EH-IDTBR** blend increased the PCE by 17%, from 7.82% to 9.19%. This improvement in PCE is mainly due to the increase in the short circuit current density and the fill factor of the ternary blend solar cells. The EQE spectra shown in (Fig. 5(d)), for the ternary blend compared to the binary **PTB7-Th:EH-IDTBR** imply that the ternary component is not only enhancing the absorption in the wavelength region below 500 nm, but also playing other functions to improve the solar cell device performance which will be further discussed in a later section.

With the success of **EH-5T-TTC** as a ternary component in two non-fullerene based acceptor systems, the influence of **EH-5T-TTC** as a ternary component in **PTB7-Th:PC$_{71}$BM** blend was investigated. The absorption spectra of the **PTB7-Th:PC$_{71}$BM** and the **EH-5T-TTC:PTB7-Th:PC$_{71}$BM** blend systems are shown in Fig. S4(a).† The addition of 10 wt% of **EH-5T-TTC** to the binary blend of **PTB7-Th:PC$_{71}$BM** mainly enhances the absorption in the spectral range below 550 nm. Photovoltaic performance studies were conducted with and without 1,8-diiodooctane (DIO) in the blend systems, which is often used as an additive in OPVs and acts as a co-solvent and plasticiser to give varying morphologies in blends.[24] The corresponding device performance parameters for the various blends are listed in Table S2† and the effect of **EH-5T-TTC** in the presence of DIO on the *J*–*V* characteristics is shown in Fig. S5.† When DIO is present, the incorporation of **EH-5T-TTC** to the **PTB7-Th:PC$_{71}$BM** blend does not result in an increase in PCE compared to the binary blend. However without the presence of DIO in the binary blend of **PTB7-Th:PC$_{71}$BM**, the incorporation of 10 wt% **EH-5T-TTC** increased the PCE by 85% (from 3.3% to 6.3%). The corresponding *J*–*V* characteristics are shown in Fig. S4(c)† and the photovoltaic performance parameters are summarised in Table S2.† The main photovoltaic performance factors that are improved by the incorporation of 10 wt% **EH-5T-TTC** are short circuit current density and FF. This increase in J_{SC} is in line with the increase in EQE as shown in Fig. S4(d).† Also as seen from Fig. S4(d) and (a),† the absorbance of the ternary blend and the external quantum efficiency (EQE) spectra show enhancement in the same spectral region, implying enhanced light harvesting by the ternary blend compared to the binary blend. Table 1 summarises how the incorporation of **EH-5T-TTC** enhances the

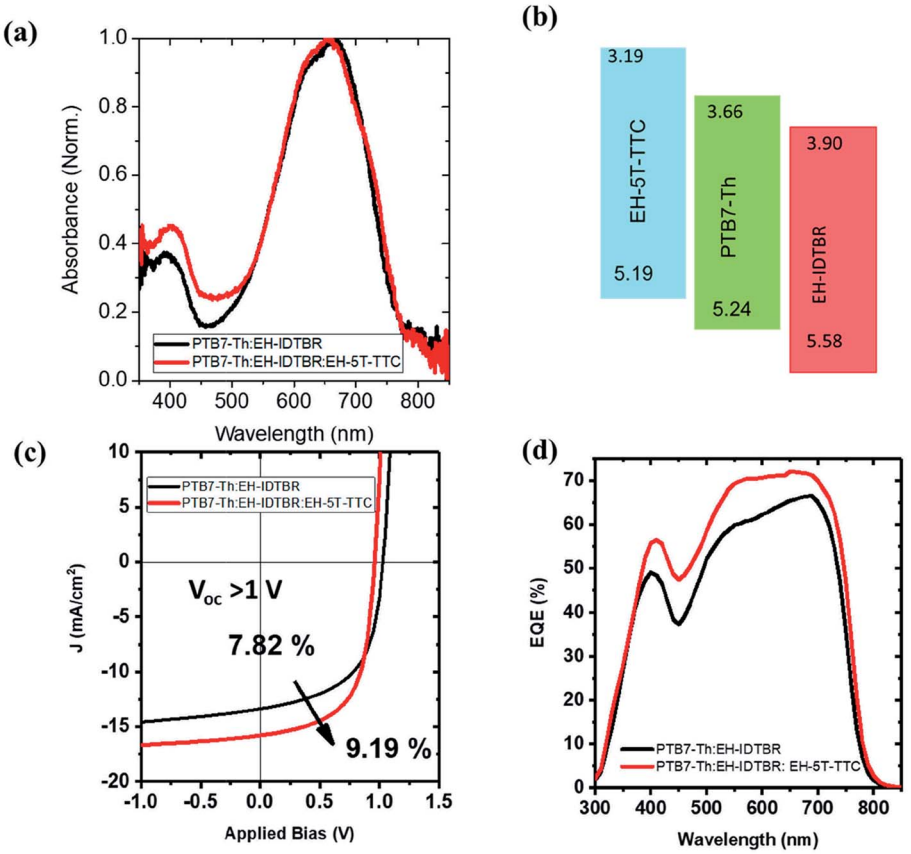

Fig. 5 (a) Absorption spectra of the binary PTB7-Th:EH-IDTBR and ternary PTB7-Th:EH-IDTBR:EH-5T-TTC blends; (b) energy level diagram of the three components in the blend system; (c) *J*–*V* characteristics of the best binary and ternary OPV devices; (d) comparison of the EQE spectra of the binary and ternary blend systems.

photovoltaic properties of different binary blends. So far the role of ternary component **EH-5T-TTC** in the UV-vis absorption properties and the photovoltaic properties of the **PTB7-Th**:fullerene/non-fullerene blend with and without **EH-5T-TTC** were discussed. Now, in the following section the reasons for the improved photovoltaic properties of the ternary blend are discussed.

Discussion

To understand why **EH-5T-TTC** enhances the power conversion efficiency of **PTB7-Th**:fullerene/non-fullerene based blends, various microstructural and optical characterisations were performed. The recombination dynamics of the charge carriers at the open circuit and short circuit current density conditions were investigated by studying the photovoltaic performance as a function of the intensity of incident light. The short circuit current density J_{SC} depends upon the light intensity I by a power law relation of

$$J_{SC} \propto I^{\alpha}$$

where α is recombination factor and is unity when all the separated charges are collected to the electrodes. A small decrease of α from unity corresponds to weak bi-molecular recombination losses, whereas the values of α in the range of 0.7–0.8 correspond to space charge effects.[25,26] The variation of J_{SC} as a function of light intensity (log–log scale) for the blends of **PTB7-Th:PC$_{71}$BM**, and **PTB7-Th:EH-IDTBR** with and without the ternary component **EH-5T-TTC** is shown in Fig. 6(a) and (b). In the case of ternary blends with non-fullerene acceptors, under short circuit current density, the introduction of **EH-5T-TTC** does not contribute to the reduction of bimolecular recombination (Fig. 6(b)). Solar cells based on both binary and ternary blends showed a weak bimolecular recombination at short circuit conditions with α values of ~0.97 for both blends. This implies that most of the charges generated at the short circuit conditions are swept out of the active layer to constitute current in the external circuit in both cases. So, measurements of the dependence of J_{SC} on light intensity for the ternary blend with the non-fullerene acceptor suggest that bimolecular recombination plays a minor role to account for the improved OPV performance. Similar results are observed for binary and ternary blends of **PTB7-Th:ITIC** (Fig. S6†). However, in the case of the blends with fullerene acceptors (**PTB7-Th:PC$_{71}$BM**), the α value is increased from 0.97 to 1.0 due to the incorporation of the **EH-5T-TTC** implying that the incorporation of the ternary component reduced the bimolecular recombination losses.

Table 1 A summary table showing the photovoltaic performance parameters of the binary and ternary blends (containing the optimised amount of EH-5T-TTC)

Blend composition	Binary/ternary	J_{SC} (mA cm^{-2})	V_{OC} (V)	FF (%)	PCE (%) avg.	PCE best (%)
PTB7-Th:ITIC	Binary	13.5 ± 0.5	0.804 ± 0.005	65.5 ± 0.3	7.08 ± 0.20	7.26
	Ternary	14.9 ± 0.4	0.788 ± 0.005	64.3 ± 0.3	7.56 ± 0.17	7.74
PTB7-Th:EH-IDTBR	Binary	12.81 ± 0.3	1.02 ± 0.01	56.7 ± 0.5	7.46 ± 0.17	7.82
	Ternary	15.35 ± 0.4	0.965 ± 0.005	59.7 ± 0.8	8.84 ± 0.27	9.19
PTB7-Th:PC$_{71}$BM	Binary	11.4 ± 0.3	0.770 ± 0.009	36.5 ± 0.4	3.2 ± 0.1	3.36
	Ternary	15.0 ± 0.2	0.778 ± 0.004	52.0 ± 0.6	6.09 ± 0.24	6.31

To gain further information about recombination mechanisms, the variation of V_{OC} as a function of light intensity was studied. V_{OC} is related to the incident light intensity through the relation: $V_{OC} = n\frac{k_B T}{q}\ln(I) + \text{constant}$, where k_B is the Boltzmann constant, n is the ideality factor, q is the charge and T is the temperature. When the slope of V_{OC} *versus* the logarithm of the light intensity is $\frac{k_B T}{q}(n \sim 1)$, the recombination mechanism that dominates is bimolecular recombination. A stronger dependence of V_{OC} on light intensity corresponding to ($n > 1$) indicates the presence of Shockley–Read–Hall (SRH) or trap assisted recombination competing with bimolecular recombination. In the case of binary and ternary blends with non-fullerene acceptors, the n values are similar and close to 1 implying that incorporation of **EH-5T-TTC** is not contributing towards the reduction of trap-assisted recombination losses [Fig. 6(c), (d) and S6(b)†]. However, for the blends with the fullerene acceptor as shown in Fig. 6(c), the variation of V_{OC} with incident light intensity implies that under open circuit conditions, in the presence of **EH-5T-TTC**, the n value has come down from 1.4 to 1.2 indicating that trap-assisted recombination losses are reduced for the fullerene-based ternary blend.

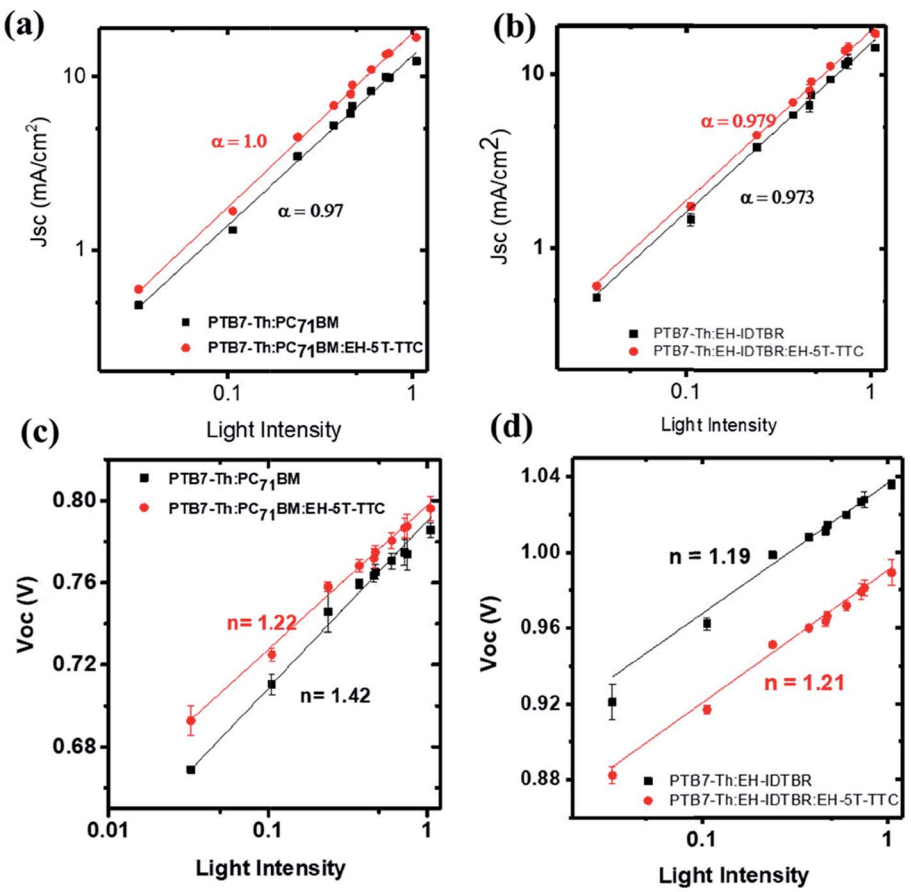

Fig. 6 Variation of J_{SC} and V_{OC} as a function of light intensity for binary and ternary blends of PTB7-Th:PC$_{71}$BM [(a) and (c)] and PTB7-Th:EH-IDTBR [(b) and (d)].

To understand the differences in recombination dynamics of the blends containing **EH-5T-TTC** and fullerene/non-fullerene acceptors, detailed morphological characterisation was performed using atomic force microscopy (AFM). AFM height images of the binary blends (**PTB7-Th:EH-IDTBR** and **PTB7-Th:$PC_{71}BM$**) and their ternary blends with **EH-5T-TTC** are shown in Fig. 7(a)–(d). The corresponding AFM height images for **PTB7-Th:ITIC** blends are shown in Fig. S7.† In the case of blends based on the non-fullerene acceptors, incorporation of **EH-5T-TTC** did not make any change in the domain size, but the appearance of self-assembled percolated structures could be observed. This type of percolated pathway, which enhances the charge transport properties of the material, is more obvious for **PTB7-Th:EH-IDTBR** (Fig. 7(a) and (b)) compared to **PTB7-Th:ITIC** (Fig. S7†). This could be the reason for the improved fill factor for the ternary blend **EH-5T-TTC:PTB7-Th:EH-IDTBR** based solar cells, compared to the binary **PTB7-Th:EH-IDTBR** blend as shown in Table S1.† Also the root mean square (RMS) roughness values of the binary blends with non-fullerene acceptors are not changed much due to the incorporation of **EH-5T-TTC**. In contrast to this, in the case of fullerene-based blends of **PTB7-Th:$PC_{71}BM$**, the incorporation of **EH-5T-TTC** brings a dramatic drop in the domain size and reduces the RMS roughness from 1.8 nm to 0.84 nm, similar to the effect of DIO as additive [Fig. 7(c) and (d)]. This finer morphology of the **PTB7-Th:$PC_{71}BM$:EH-5T-TTC** ternary blend compared to **PTB7-Th:$PC_{71}BM$** can explain the reduced recombination losses of the ternary compared to the binary blend. The difference in morphology observed between fullerene and non-fullerene based blends upon the incorporation of **EH-5T-TTC** can account for the variation in recombination dynamics detailed above.

To understand the role of surface energy as the driving force for the difference in morphology for fullerene and non-fullerene based ternary blends containing **EH-5T-TTC**, contact angle measurements were performed. Previous studies have shown that the surface energy of different components in a blend determines their segregation and location in the blend system.[27,28] The contact angles of polymer **PTB7-Th**, fullerene acceptor **$PC_{71}BM$**, non-fullerene acceptors **EH-IDTBR** and **ITIC**, and the ternary component **EH-5T-TTC** were measured to evaluate the surface energy (Fig. S8† and Table 2). The contact angles were measured with water, ethylene glycol and diiodomethane. The surface energy is calculated using the Owens and Wendt equation (eqn (1)), corresponding to three different solvents: deionised water, diiodomethane and ethylene glycol.[27,29–31] The estimated surface energy values are shown in Table 2.

$$\sigma_L \frac{(1+\cos\theta)}{2\sqrt{\sigma_L^d}} = \sqrt{\sigma_S^p}\sqrt{\frac{\sigma_L^p}{\sigma_L^d}} + \sqrt{\sigma_S^d} \quad (1)$$

In eqn (1), θ is the contact angle, σ_L and σ_S are the liquid and solid surface tension, respectively. The addition of d and p in the superscript refer to the dispersive and polar components of each solvent. The calculated surface energy values of **PTB7-Th**, **EH-5T-TTC**, and the non-fullerene acceptors **ITIC** and **EH-IDTBR** are closely matching and in the range of 18–20 mJ m^{-2}. The small difference in surface energy between the blend components results in a well-mixed morphology and the same reason can account for the similar morphology for binary and ternary blends containing non-fullerene acceptors. In the case

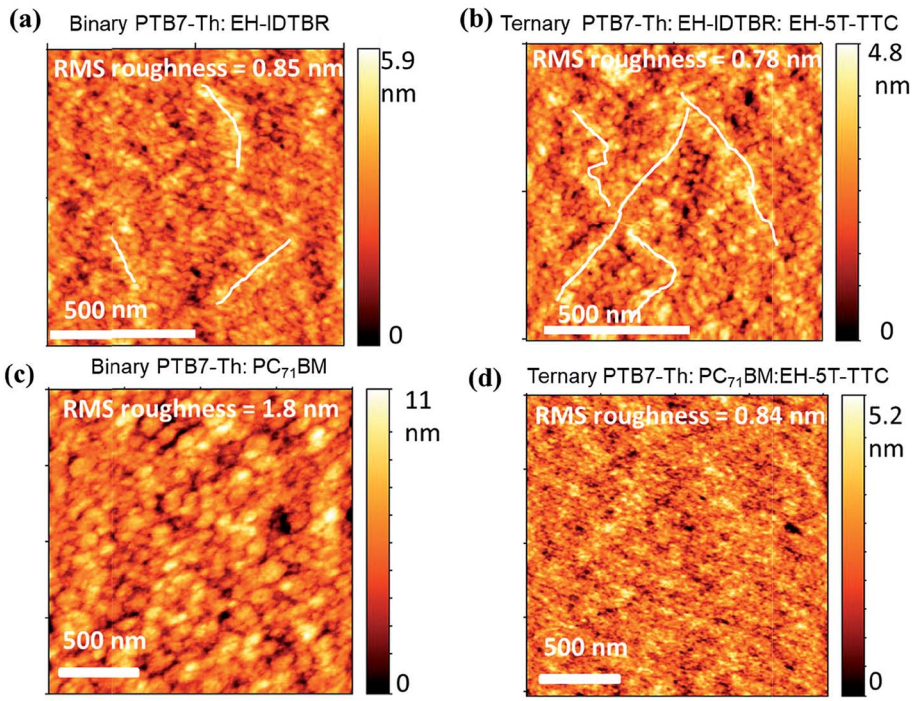

Fig. 7 AFM height images of the binary and ternary blends of PTB7-Th:EH-IDTBR and PTB7-Th:$PC_{71}BM$. (a) Binary PTB7-Th:EH-IDTBR (b) ternary PTB7-Th:EH-IDTBR:EH-5T-TTC (c) binary PTB7-Th:PC71BM and (d) ternary PTB7-Th:$PC_{71}BM$:EH-5T-TTC.

Table 2 Surface energy values of the donor and acceptor materials studied in this work

Material	Surface energy (mJ m^{-2})
PTB7-Th	19.7
EH-5T-TTC	20.4
$PC_{71}BM$	32.1
ITIC	19.5
EH-IDTBR	18.3

of the **PTB7-Th:$PC_{71}BM$** blend, the surface energy of **$PC_{71}BM$** (32.1 mJ m^{-2}) is higher than for **PTB7-Th** (19.7 mJ m^{-2}) and this large difference in surface energy results in a phase separated morphology with large domains. However, with the incorporation of **EH-5T-TTC** (20.4 mJ m^{-2}) a well-mixed morphology is observed for the **EH-5T-TTC:PTB7-Th:PC71BM** blend, implying that the thermodynamic driving force for phase separation of **PTB7-Th** and **$PC_{71}BM$** has been reduced by the ternary component.

After identifying the role of **EH-5T-TTC** in the morphology of each ternary blend compared to the binary blend containing fullerene and non-fullerene acceptors, the contribution of this altered morphology towards the photogeneration process was studied by the photocurrent analysis method. The role of **EH-5T-TTC** in the enhanced photocurrent is investigated by considering the charge generation and exciton dissociation processes in the binary and ternary blends by determining the saturation current density (J_{sat}) and exciton dissociation probabilities $P(E,T)$ of the respective blends. Fig. 8 shows the photocurrent density (J_{ph}) *vs.* effective voltage (V_{eff}) characteristics for the **PTB7-Th:ITIC**, **PTB7-Th:EH-IDTBR** and **PTB7-Th:$PC_{71}BM$** blends compared to their respective ternary blend with **EH-5T-TTC**. J_{ph} is obtained using the following relation:[32,33]

$$J_{ph} = J_L - J_D$$

where J_L and J_D are the photocurrent densities under illumination and in the dark, respectively, and V_{eff} is determined using $V_{eff} = V_0 - V_a$ where V_0 is the voltage at which photocurrent is zero and V_a is the applied bias voltage. As shown in Fig. 8, in the case of both fullerene and non-fullerene blends, the ternary blend has a higher photocurrent compared to the binary blend. Under high reverse bias (~4 V in this case), all the photogenerated excitons are expected to be dissociated to form free charges and the saturation current density J_{sat} is determined by the maximum exciton generation rate G_{max}. The maximum generation rate is estimated using the following relation, where e is the elementary charge and L is the thickness.[34,35]

$$J_{sat} = eG_{max} \times L$$

G_{max} values for the binary and ternary blends are listed in Fig. 8(d). With the incorporation of the ternary component **EH-5T-TTC**, the overall exciton generation rate G_{max} of the binary blend has been increased (by 5–10%). This improvement can be attributed to the increased absorption of the active layer blend due to the ternary component **EH-5T-TTC**. Thus, enhanced exciton generation was observed for **EH-5T-TTC**-added ternary components.

Along with increased exciton generation rate, exciton dissociation probability is also important for enhanced photocurrent. The exciton dissociation probability has now been estimated using the relation:

$$J_{ph} = eG_{max}P(E,T) \times L$$

where $P(E,T)$ is the dissociation probability.[34,36,37] In the case of **PTB7-Th:ITIC**, the incorporation of **EH-5T-TTC** increased the $P(E,T)$ from 81 to 91%, for **PTB7-Th:EH-IDTBR** the improvement is from 83 to 90%, and the highest improvement is obtained for **PTB7-Th:$PC_{71}BM$** where the $P(E,T)$ improvement is from 71 to 90% (Fig. S9†). This highest dissociation probability for the **PTB7-Th:$PC_{71}BM$** blend with the incorporation of **EH-5T-TTC** can be related to the finer morphology of the ternary blend compared to the binary blend system as shown in Fig. 7(c) and (d).

Finally, to investigate the possible energy transfer process between the **EH-5T-TTC** and **PTB7-Th**, steady state PL spectra were taken (Fig. S10†). The excitation wavelength used is 515 nm. No measurable PL signal could be obtained from **EH-5T-TTC**. In the case of **PTB7-Th**, the PL spectra show a broad emission peaking at 760 nm. The excitation wavelength of 515 nm used in this study excited both **PTB7-Th** and **EH-5T-TTC**. The change observed in the PL of **PTB7-Th** with 20 wt% and 40 wt% blend may be either due to reduced self-quenching upon dilution with **EH-5T-TTC** or energy transfer from **EH-5T-TTC** to **PTB7-Th**.[38]

In order to prove that the beneficial properties of **EH-5T-TTC** are unique to the core tetrathiocin structure, three types of fullerene-containing organic solar cells were prepared and characterised. The devices, which were made under the same conditions, were not optimised and the experiments were carried out simply to compare a binary device of **PTB7-Th:$PC_{71}BM$** with ternary blend devices incorporating the non-tetrathiocin compound **1** (half-unit of **EH-5T-TTC**, Scheme 2) and **EH-5T-TTC**. The highest recorded PCE of the binary device was found to be 3.33% (Table S3†). This value increased to 4.26% in **PTB7-Th:$PC_{71}BM$:1** devices, but a much greater increase was observed for the ternary blend containing **EH-5T-TTC** (5.89%). The corresponding J–V characteristics and the EQE spectra are shown in Fig. S11.† These results clearly indicate that the enhancement in device characteristics is not simply a function of the quinquithiophene chains, but is due to the physical properties of the more complex tetrathiocin structure.

So far we have shown how **EH-5T-TTC** can help with the important problem of spectral coverage in OPVs and simultaneously achieve morphology modification and energy transfer in forming an efficient ternary component in OPV blends. Now in the final section, the shelf life stability for binary and ternary blend systems has been carried out (Fig. S12†). The encapsulated solar cells were kept in ambient conditions. In the case of

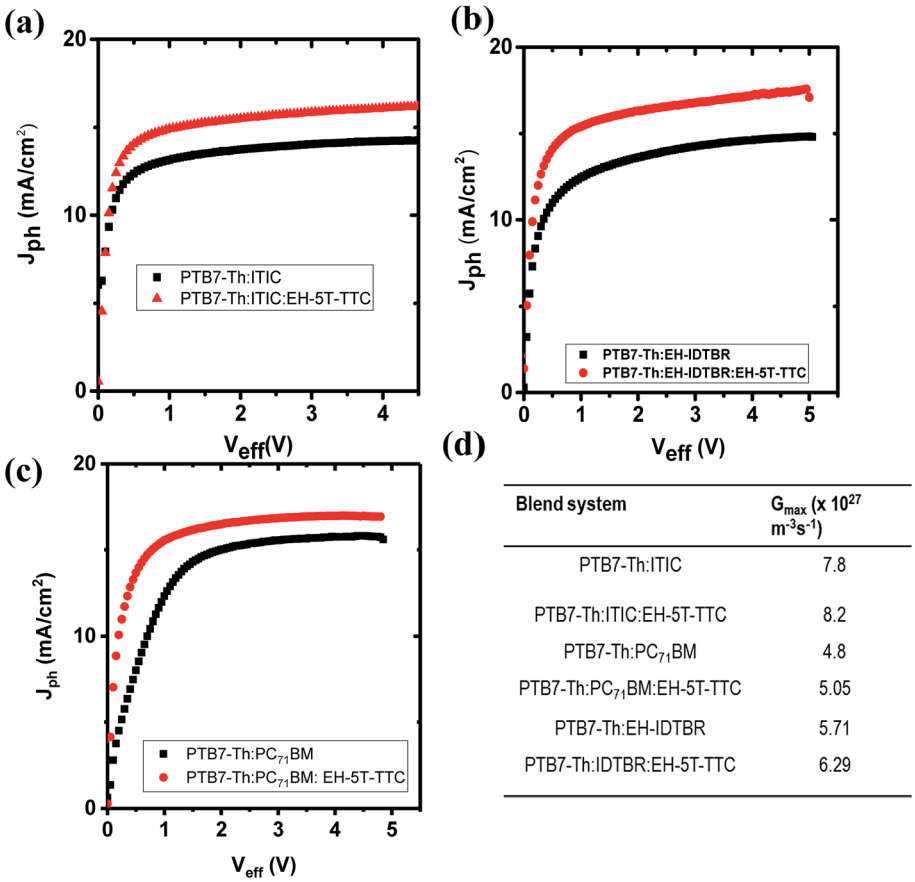

Blend system	G_{max} (x 10^{27} $m^{-3}s^{-1}$)
PTB7-Th:ITIC	7.8
PTB7-Th:ITIC:EH-5T-TTC	8.2
PTB7-Th:PC$_{71}$BM	4.8
PTB7-Th:PC$_{71}$BM:EH-5T-TTC	5.05
PTB7-Th:EH-IDTBR	5.71
PTB7-Th:IDTBR:EH-5T-TTC	6.29

Fig. 8 Comparison of photocurrent J_{ph} *vs.* V_{eff} for binary and ternary blends of (a) PTB7-Th:ITIC, (b) PTB7-Th:EH-IDTBR and (c) PTB7-Th:PC$_{71}$BM, and (d) G_{max} values for all the blends.

the ternary blend incorporating the fullerene acceptor, the shelf life study (for 6 months) has been found to be better with **EH-5T-TTC** added as a ternary component compared to DIO as the additive. This implies that in addition to the improved absorption of the visible spectral range, the incorporation of **EH-5T-TTC** can enhance the shelf-life stability compared to the commonly used DIO additive for **PTB7-Th:PC$_{71}$BM** blend.

Conclusions

We have presented a new, soluble 'double-chain' oligothiophene compound (**EH-5T-TTC**), based on two quinquithiophene units bridged by a fused 8-membered tetrathiocin core. This non-conventional structure provides intermolecular contacts (π–π and S···S) in two dimensions. The synthetic strategy towards **EH-5T-TTC** is versatile and one can envisage a wide range of new fascinating conjugated structures incorporating the tetrathiocin core. We have demonstrated **EH-5T-TTC** as an efficient ternary component for both fullerene and non-fullerene based OPVs containing the efficient narrow band gap donor polymer **PTB7-Th**. The improved efficiency is mainly due to the combined effect of enhanced absorption and beneficial modification of blend morphology enhancing the photogenerated exciton generation and dissociation. A comparison of the shelf life stability studies shows that ternary blend OPVs with **EH-5T-TTC** are as stable as its binary components and in the case of the DIO-containing binary blend, the shelf life has been found to be better with **EH-5T-TTC** added as a ternary component compared to DIO as the additive.

Experimental details

Fabrication of organic solar cells

Inverted organic solar cells were fabricated on pre-patterned ITO-coated glass. The ITO-coated glass substrates were cleaned in detergent (sodium dodecyl sulfate-SDS), successively ultrasonicated in deionised water, acetone, and isopropyl alcohol, and exposed to Plasma Asher for 3 minutes. The **PTB7-Th:PC$_{71}$BM** blend solutions were prepared by dissolving the components in a ratio of 1 : 1.5 (by weight), with a total concentration of 25 mg mL^{-1} in chlorobenzene, with and without 3 vol% DIO. The solution was kept stirring at 60 °C for ~8 h before spin-coating.

In the case of **PTB7-Th:ITIC** blend solution was prepared by mixing 1 : 1.3 (wt%) donor to acceptor with a total concentration of 25 mg mL^{-1} in chlorobenzene solvent. For **PTB7-Th:EH-IDTBR** blend, the donor and acceptor weight ratio was 1 : 1 with a total concentration of 20 mg mL^{-1} in *o*-dichlorobenzene (*o*DCB) solvent. The blend solutions were kept stirring at 60 °C for ~6 hours before spin coating. In all the inverted organic solar cells

fabricated, the electron transporting layer was amorphous ZnO (a-ZnO) thin film having thickness ~25 nm and was prepared according to a previous report.[39] The active layer was deposited by spin-coating (1000 rpm, 60 s) on glass/ITO/a-ZnO substrates inside a nitrogen filled glove box. The samples were then transferred to a vacuum thermal evaporator (1×10^{-6} mbar base pressure) and kept under vacuum overnight before thermally evaporating the hole transporting layer of MoO_x (7 nm) and anode Ag (100 nm) using a shadow mask. The active area of the device was 0.07 cm^2. All the processing related to the active layer was performed inside a nitrogen-filled glove box.

After the electrode deposition, the devices were encapsulated with a UV optical adhesive and a glass coverslip. The current–voltage characteristics were determined under an illumination intensity of 100 mW cm^{-2} in air using an air mass 1.5 global (AM 1.5G) Sciencetech solar simulator and a Keithley 2400 source-measure unit. The illumination intensity was verified with a calibrated monosilicon detector and a KG-5 filter. The external quantum efficiency (EQE) measurements were performed at zero bias by illuminating the device with monochromatic light supplied from a Xenon arc lamp in combination with a dual-grating monochromator. The number of photons incident on the sample was calculated for each wavelength by using a silicon photodiode calibrated by the National Physical Laboratory (NPL).

Characterisation of the binary and ternary active layer blend

The surface morphology of the **PTB7-Th:$PC_{71}BM$** films was characterised using atomic force microscopy (AFM). AFM images were obtained with a Bruker MultiMode 8 instrument in the tapping mode. NANOSENSORS™ PPP-NCSTR Si cantilever tips with force constant of 6–7 Nm^{-1} were used as AFM probes. Steady state absorption spectra of the blend films were recorded using a Cary 300 spectrometer for the wavelength range of 300–800 nm. For this, the active layer blend was deposited under identical conditions to that used for OPV devices on a quartz disc. Steady state PL spectra were measured with a Hamamatsu streak camera C10910-05 with S-20ER photocathode and 650 nm as excitation wavelength from an optical parametric amplifier pumped by Pharos laser (from Light Conversion). To measure the contact angle, a goniometer was used with angles estimated by eye using the built-in protractor.

Conflicts of interest

There are no conflicts to declare.

Acknowledgements

We thank the EPSRC for funding under grants EP/L012200/1 and EP/L012294/1.

References

1 *Nanostructured Materials for Type III Photovoltaics*, ed. P. J. Skabara and M. A. Malik, RSC Publishing, Cambridge, 2017.
2 K. Hongkyu, K. Geunjin, K. Junghwan, K. Sooncheol, K. Heejoo and L. Kwanghee, *Adv. Mater.*, 2016, **28**, 7821–7861.
3 D. Baran, R. S. Ashraf, D. A. Hanifi, M. Abdelsamie, N. Gasparini, J. A. Röhr, S. Holliday, A. Wadsworth, S. Lockett, M. Neophytou, C. J. M. Emmott, J. Nelson, C. J. Brabec, A. Amassian, A. Salleo, T. Kirchartz, J. R. Durrant and I. McCulloch, *Nat. Mater.*, 2016, **16**, 363–369.
4 S. Chen, Y. Liu, L. Zhang, P. C. Y. Chow, Z. Wang, G. Zhang, W. Ma and H. Yan, *J. Am. Chem. Soc.*, 2017, **139**, 6298–6301.
5 J. L. Krishnan, M. Al-Senani, A. El-Labban, I. Gereige, G. O. Ngongang_Ndjawa, J. C. D. Faria, T. Kim, K. Zhao, F. Cruciani, D. H. Anjum, M. A. McLachlan, P. M. Beaujuge and A. Amassian, *Adv. Energy Mater.*, 2015, **5**, 1500204.
6 H.-C. Liao, C.-C. Ho, C.-Y. Chang, M.-H. Jao, S. B. Darling and W.-F. Su, *Mater. Today*, 2013, **16**, 326–336.
7 A. Wadsworth, R. S. Ashraf, M. Abdelsamie, S. Pont, M. Little, M. Moser, Z. Hamid, M. Neophytou, W. Zhang, A. Amassian, J. R. Durrant, D. Baran and I. McCulloch, *ACS Energy Lett.*, 2017, **2**, 1494–1500.
8 Z. Wenchao, L. Sunsun, Z. Shaoqing, L. Xiaoyu and H. Jianhui, *Adv. Mater.*, 2017, **29**, 1604059.
9 C. Winder and N. S. Sariciftci, *J. Mater. Chem.*, 2004, **14**, 1077–1086.
10 B. Minnaert and P. Veelaert, *Materials*, 2012, **5**, 1933–1953.
11 X. Liu, Y. Yan, Y. Yao and Z. Liang, *Adv. Funct. Mater.*, 2018, **28**, 1802004.
12 N. Gasparini, A. Salleo, I. McCulloch and D. Baran, *Nat. Rev. Mater.*, 2019, **4**, 229–242.
13 Q. Jiang, L. Zhang, H. Wang, X. Yang, J. Meng, H. Liu, Z. Yin, J. Wu, X. Zhang and J. You, *Nat. Energy*, 2016, **2**, 16177.
14 L. Lu, M. A. Kelly, W. You and L. Yu, *Nat. Photonics*, 2015, **9**, 491–500.
15 Y. Yang, W. Chen, L. Dou, W.-H. Chang, H.-S. Duan, B. Bob, G. Li and Y. Yang, *Nat. Photonics*, 2015, **9**, 190–198.
16 P. P. Khlyabich, A. E. Rudenko, R. A. Street and B. C. Thompson, *ACS Appl. Mater. Interfaces*, 2014, **6**, 9913–9919.
17 P. P. Khlaybich, A. E. Rudenko, B. C. Thompson and L. Yueh-Lin, *Adv. Funct. Mater.*, 2015, **25**, 5557–5563.
18 J. Mai, T.-K. Lau, J. Li, S.-H. Peng, C.-S. Hsu, U. S. Jeng, J. Zeng, N. Zhao, X. Xiao and X. Lu, *Chem. Mater.*, 2016, **28**, 6186–6195.
19 I. A. Wright, A. L. Kanibolotsky, J. Cameron, T. Tuttle, P. J. Skabara, S. J. Coles, C. T. Howells, S. A. J. Thomson, S. Gambino and I. D. W. Samuel, *Angew. Chem., Int. Ed.*, 2012, **51**, 4562–4567.
20 P. J. Skabara, I. M. Serebryakov, D. M. Roberts, I. F. Perepichka, S. J. Coles and M. B. Hursthouse, *J. Org. Chem.*, 1999, **64**, 6418–6424.
21 I. A. Wright, P. J. Skabara, J. C. Forgie, A. L. Kanibolotsky, B. Gonzalez, S. J. Coles, S. Gambino and I. D. W. Samuel, *J. Mater. Chem.*, 2011, **21**, 1462–1469.
22 S. Ralf, *Angew. Chem., Int. Ed. Engl.*, 1975, **14**, 655–664.
23 P. J. Skabara, J. B. Arlin and Y. H. Geerts, *Adv. Mater.*, 2013, **25**, 1948–1954.
24 Y. Zhang, A. J. Parnell, F. Pontecchiani, J. F. K. Cooper, R. L. Thompson, R. A. L. Jones, S. M. King, D. G. Lidzey and G. Bernardo, *Sci. Rep.*, 2017, **7**, 44269.

25 S. R. Cowan, A. Roy and A. J. Heeger, *Phys. Rev. B: Condens. Matter Mater. Phys.*, 2010, **82**, 245207.
26 L. J. A. Koster, V. D. Mihailetchi, R. Ramaker and P. W. M. Blom, *Appl. Phys. Lett.*, 2005, **86**, 3.
27 J.-H. Huang, Y.-S. Hsiao, E. Richard, C.-C. Chen, P. Chen, G. Li, C.-W. Chu and Y. Yang, *Appl. Phys. Lett.*, 2013, **103**, 043304.
28 S. Honda, H. Ohkita, H. Benten and S. Ito, *Adv. Energy Mater.*, 2011, **1**, 588–598.
29 R. L. Bendure, *J. Colloid Interface Sci.*, 1973, **42**, 137–144.
30 S. Siboni, C. Della Volpe, D. Maniglio and M. Brugnara, *J. Colloid Interface Sci.*, 2004, **271**, 454–472.
31 D. Y. Kwok and A. W. Neumann, *Adv. Colloid Interface Sci.*, 1999, **81**, 167–249.
32 P. W. M. Blom, V. D. Mihailetchi, L. J. A. Koster and D. E. Markov, *Adv. Mater.*, 2007, **19**, 1551–1566.
33 L. Yang, J. R. Tumbleston, H. Zhou, H. Ade and W. You, *Energy Environ. Sci.*, 2013, **6**, 316–326.
34 V. Shrotriya, Y. Yao, G. Li and Y. Yang, *Appl. Phys. Lett.*, 2006, **89**, 063505.
35 P. Gautam, R. Sharma, R. Misra, M. L. Keshtov, S. A. Kuklin and G. D. Sharma, *Chem. Sci.*, 2017, **8**, 2017–2024.
36 V. D. Mihailetchi, L. J. A. Koster, J. C. Hummelen and P. W. M. Blom, *Phys. Rev. Lett.*, 2004, **93**, 216601.
37 N. Bauer, Q. Zhang, J. Zhao, L. Ye, J.-H. Kim, I. Constantinou, L. Yan, F. So, H. Ade, H. Yan and W. You, *J. Mater. Chem. A*, 2017, **5**, 4886–4893.
38 S. M. Menke, W. A. Luhman and R. J. Holmes, *Nat. Mater.*, 2012, **12**, 152.
39 L. K. Jagadamma, M. Abdelsamie, A. El Labban, E. Aresu, G. O. Ngongang Ndjawa, D. H. Anjum, D. Cha, P. M. Beaujuge and A. Amassian, *J. Mater. Chem. A*, 2014, **2**, 13321–13331.